J. Webster (ed.), *Wiley Encyclopedia of Electrical and Electronics Engineering*

PULSE COMPRESSION

Ultrashort pulse technology has made it possible to reach ultrahigh peak powers, in pulses of modest energy. Current techniques to generate millijoules of femtosecond radiation are however rather complex and expensive. The most common technique (1) is to use a femtosecond Ti:sapphire laser [requiring a rather expensive pump source—either an argon laser or a frequency-doubled diode-pumped Nd:YVO_4 (Neodymium doped Yttrium Orthovanadate) laser] followed by a regenerative amplifier. To avoid laser-induced damage through self-focusing in the components of the amplifer, the pulse to be amplified is stretched several thousand times by a pair of gratings. After amplification, the stretching process is reversed in a compressor. The overall source consists thus of a pump laser, an oscillator, an isolator, a stretcher, a regenerative amplifier with its pump laser [generally a *Q*-switched Nd:YAG (Neodymium doped Yttrium Aluminum Garnet) laser], eventually a postamplifier, and finally a compressor.

One of the long term goals of pulse compression through type II second harmonic generation is to design a cheaper, compact alternative to these large high-power systems, with a flashlamp-pumped Nd:YAG laser as the source of energy. The Nd:YAG laser has been the workhorse of industrial applications with lasers for a couple of decades. It may become the most economical source of femtosecond pulses as well.

Pulses of 40 ps to 100 ps duration are routinely generated by mode-locked commercial Nd:YAG lasers. The implementation of negative feedback has made it possible to decrease the pulse duration to 10 ps, and the pulse-to-pulse energy fluctuations to less than 1%. Implementation of passive negative feedback involves simply inserting a two-photon absorbing wafer (0.4 mm to 1 mm thickness) and an aperture in the resonator (2). Various semiconductors have been investigated as two-photon absorbers (3,4). The combination of a two-photon absorber and an aperture acts as an energy limiter (5). As the intracavity pulse energy increases to a steady-state value, the two-photon phtocarriers create a negative lens in the material, which will defocus the remaining part of the pulse. As a result, at each round trip, the pulse is compressed through clipping of its tail, and the pulse energy is limited to a fixed value (6). After amplification, pulses of 10 ps duration and hundreds of millijoules of energy are routinely generated at 1.064 μm.

This article addresses the first step towards the creation of a multiple-wavelength femtosecond source, based on a Nd:YAG laser. The basic principle is to exploit frequency conversion and parametric generation in a nonlinear crystal, in order to reach other wavelengths and generate shorter pulses. The picosecond pulses generated by the infrared laser have sufficiently high peak intensity to be an ideal source for harmonic conversion through nonlinear optics. Because their nonlinearity is electronic and nonresonant, harmonic-generating crystals respond instantaneously (in the order of less than 1 fs) on the time scale of the shortest optical pulse. There appears to be no limit to the palette of frequencies that can be generated through nonlinear optics, from dc (optical rectification) to infrared (difference-frequency generation and optical parametric generation and amplification), to visible, and to UV (sum-frequency generation). The shorter the pulse, the higher the peak intensity for a given pulse energy (and thus the more efficient the nonlinear process). There is however an insidious problem that plagues nonlinear optics with ultrashort pulses: the velocity of a wave packet is not the same as that of the individual waves. In second harmonic generation, even though the fundamental and second

harmonic waves are *phase-matched* (i.e., these waves propagate at the same wave velocity), the fundamental pulse propagates at a different velocity (in general faster) than the second harmonic pulse.

This effect, generally called group-velocity dispersion, appears to be the nemesis of most frequency mixing schemes. In general, because of group-velocity dispersion, the second harmonic will propagate more slowly than the fundamental that feeds it. Therefore, the nonlinear interaction between two pulses of duration τ at frequencies ω_1 and ω_2 is limited to the walk-off distance:

$$L = \frac{\tau}{\dfrac{1}{v_{g1}} - \dfrac{1}{v_{g2}}} \qquad (1)$$

where v_{g1} and v_{g2} are the group velocities at their respective wavelengths. For instance, in type I interaction, the second harmonic of 744 nm radiation in potassium dihydrogen phosphate (KH_2PO_4 or KDP) is delayed with respect to the fundamental by 80 fs/mm. The relative delay is much larger in BBO (β-BaB_2O_4) (240 fs/mm). Therefore, very thin (<1 mm) crystals are generally selected for all nonlinear mixing processes involving femtosecond pulses. It has been shown however that group-velocity dispersion, combined with amplitude modulation associated with the depletion of the fundamental waves, can lead to efficient pulse compression (7,8). Small amounts of compression were first demonstrated with subpicosecond pulses (9,10). Subsequently, pulse compression through second harmonic generation in very long (5 cm to 6 cm) KDP and deuterated KDP (KD_2PO_4 or KD∗P) crystals was predicted (8) and demonstrated (11). It should be noted that a similar compression mechanism has been investigated in synchronously pumped optical parametric oscillators (12,13,14,15).

A Simple Model of Pulse Compression in Harmonic Generation

In the following, we assume second harmonic generation of type II, with the group velocity of the second harmonic (an extraordinary wave) intermediate between that of the ordinary o and extraordinary e fundamental waves. Let us take as an example second harmonic generation of a 10 ps Nd:YAG laser pulse in a KDP crystal of thickness d. Generalization to other systems will be discussed later. Let us consider two fundamental pulses at 1.064 μm, and a second harmonic e wave that has been generated by the nonlinear polarization $P_{\mathrm{e,NL}} = \epsilon_0 \chi^{(2)} E_\mathrm{o} E_\mathrm{e}$, where $E_j = \mathscr{E}_j \exp i(\omega t - k_j z)$ (j = o, e) are the electric fields of the ordinary and extraordinary fundamental waves, and $\chi^{(2)}$ is the second-order nonlinear susceptibility. The wave vectors of the ordinary and extraordinary fundamental waves are $k_\mathrm{o} = \omega n_\mathrm{o}(\omega)/c$ and $k_\mathrm{e} = \omega n_\mathrm{e}(\omega)/c$, and for the second harmonic wave $k_2 = \omega_2 n_2(\omega_2)/c$; $n_\mathrm{o}(\omega)$, $n_\mathrm{e}(\omega)$, and $n_2(\omega_2)$ are the refractive indexes of the nonlinear crystal. This nonlinear polarization generates a second harmonic field as an extraordinary wave $E_2 = \mathscr{E}_2 \exp i(\omega_2 t - k_2 z)$ at the frequency $\omega_2 = 2\omega$. The propagating second harmonic will remain in phase with the second harmonic generated at any point z in the crystal if the *phase-matching* condition is satisfied:

$$k_2 = k_\mathrm{o} + k_\mathrm{e} \qquad (2)$$

This phase-matching condition is satisified if the crystal orientation is chosen such that

$$n_2 = \frac{n_\mathrm{o} + n_\mathrm{e}}{2} \qquad (3)$$

The phase-matching condition implies that the *phase velocities* are matched. After a propagation length L through the crystal, the phase delay of the second harmonic $L/v_{\mathrm{p},2}$ is equal to the sum of the phase delay of the

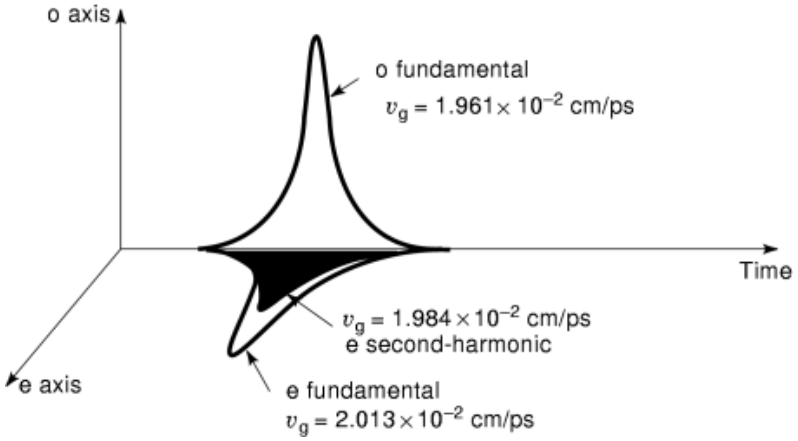

Fig. 1. As an e and an o pulse enter the crystal, they generate a second harmonic pulse with intensity proportional to the product of the two fundamental pulse intensities. The three pulses will eventually split, since they propagate in the crystal with different group velocities.

two fundamentals $L/v_{\mathrm{p,o}} + L/v_{\mathrm{p,e}}$. The phase velocities are defined as

$$\begin{aligned} v_{\mathrm{p},2} &= \frac{c}{n_{\mathrm{e}}(\omega_2)} \\ v_{\mathrm{p,o}} &= \frac{c}{n_{\mathrm{o}}(\omega)} \\ v_{\mathrm{p,e}} &= \frac{c}{n_{\mathrm{e}}(\omega)} \end{aligned} \tag{4}$$

The fact that the waves remain in phase does not necessarily imply that *pulses* reach the end of the crystal simultaneously. The three wave packets propagate at the *group velocities* given by

$$\begin{aligned} \frac{1}{v_{\mathrm{g},2}} &= \frac{1}{c}\left[n_{\mathrm{e}}(\omega_2) - \lambda \frac{dn_{\mathrm{e}}}{d\lambda}\bigg|_{\omega_2}\right] \\ \frac{1}{v_{\mathrm{g,o}}} &= \frac{1}{c}\left[n_{\mathrm{o}}(\omega) - \lambda \frac{dn_{\mathrm{o}}}{d\lambda}\bigg|_{\omega}\right] \\ \frac{1}{v_{\mathrm{g,e}}} &= \frac{1}{c}\left[n_{\mathrm{e}}(\omega) - \lambda \frac{dn_{\mathrm{e}}}{d\lambda}\bigg|_{\omega}\right] \end{aligned} \tag{5}$$

If a fundamental pulse with an e and an o component enters the crystal, it will generate a second harmonic pulse, which will propagate at a different group velocity than either component of the fundamental. The three pulses with different group velocities are shown in Fig. 1.

The velocity of the second harmonic is intermediate between that of the two fundamentals. Let us consider the case where the fundamental e wave enters the crystal *delayed* with respect to the fundamental o wave. A second harmonic will be generated at the temporal overlap between the two pulses, as sketched in Fig. 2(a). In a frame of reference moving at the group velocity of the second harmonic, the two fundamental pulses will travel

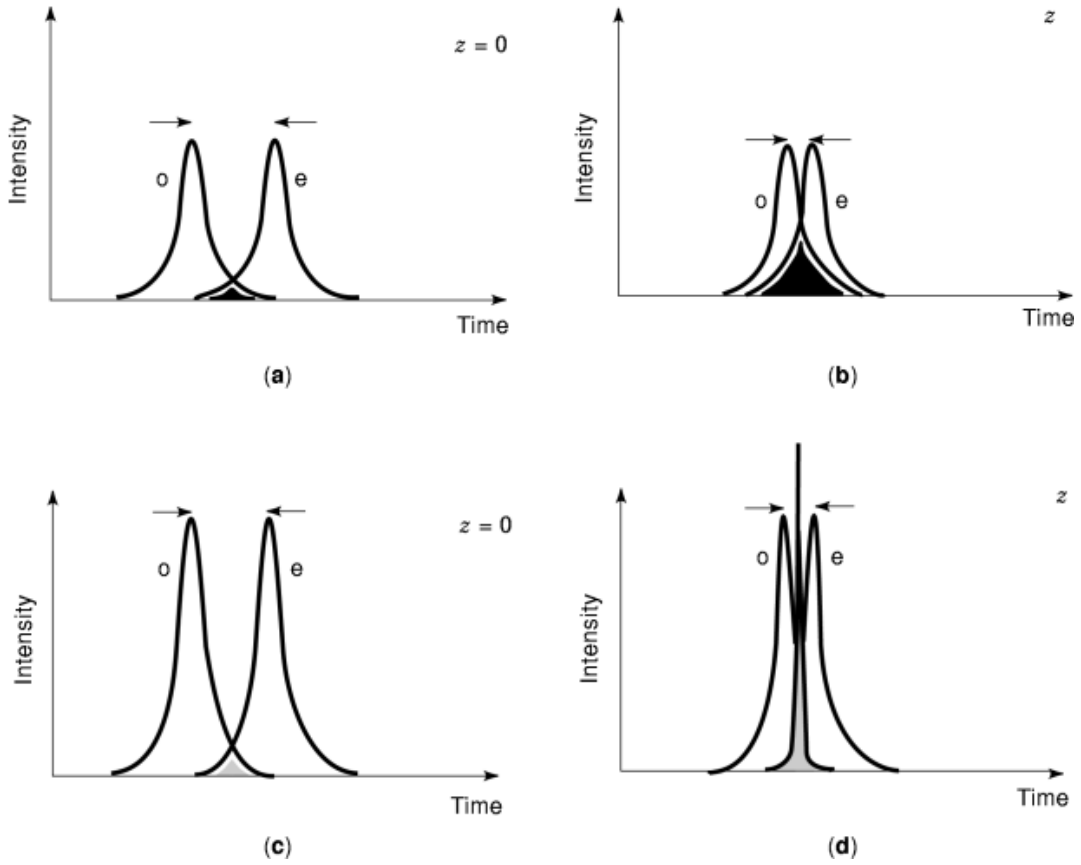

Fig. 2. The three pulses are represented in a temporal frame of reference moving with the group velocity of the second harmonic. Initially, at $z = 0$, the fundamental e is delayed with respect to the fundamental o wave [parts (a) and (c)]. For low input energies (a), the second harmonic will be broadened as the two fundamental pulses move into each other (b). For sufficiently high input energies (c), the overlap between the two fundamentals remains small because they are depleted by the upconversion process, and the second harmonic pulse remains short (d).

towards each other (since the faster e wave has been delayed). After some propagation distance, the overlap of the fundamentals increases, and so does the second harmonic [Fig. 2(b)]. However, if the fundamental pulses are sufficiently intense as sketched in Fig. 2(c) and 2(d), the growth of the second harmonic may be so fast as to deplete the fundamentals. As a result, the spatial overlap of the two fundamentals remains small, as they move into each other [Fig. 2(d)].

Crude order-of-magnitude estimates of the power required can be made by considering square fundamental pulses (temporal profile). Let us assume first that the group velocity of the second harmonic is exactly the average of the group velocities of the extraordinary and ordinary fundamentals. If, as in Fig. 2(a), the two fundamental pulses are given a predelay, they will move across each other, in a frame of reference moving with the second harmonic, as they propagate through the crystal. One expects also that the second harmonic pulse will be even longer than the fundamental. At perfect phase matching, the second harmonic generated after a

distance z is given by (16)

$$\mathscr{E}_2(z) = \mathscr{E}(0)\tanh\frac{z}{L_{\mathrm{sh}}} \tag{6}$$

where, at $z = 0$, $\mathscr{E}_{\mathrm{o}} = \mathscr{E}_{\mathrm{e}} = \mathscr{E}$, and the characteristic distance L_{sh} is given by

$$\frac{1}{L_{sh}} = \frac{\omega\chi^{(2)}}{n_2 c}\,\mathscr{E} \tag{7}$$

For optimum production of a second harmonic pulse of duration τ_{ov}, the fundamental pulses should move into each other by an overlap time τ_{ov}, over the characteristic distance L_{sh}. The condition

$$\tau_{\mathrm{ov}} = \frac{n_2 c}{\omega\chi^{(2)}\mathscr{E}}\left(\frac{1}{v_{\mathrm{g,e}}} - \frac{1}{v_{\mathrm{g,o}}}\right) \tag{8}$$

leads to an optimum intensity $I_0 = W_0/\tau_{\mathrm{ov}}$ (where W_0 is the pulse energy density over the overlap time) for the fundamental pulses. The intensity I_0 of the fundamental square pulses is given by

$$I_{\mathrm{o,e}} = \frac{\epsilon_0 c n_{\mathrm{o,e}}\mathscr{E}^2}{2} = \frac{\epsilon_0 c^3 n_{\mathrm{o,e}} n_2^2}{2(\omega\chi^{(2)}\tau_{\mathrm{ov}})^2}\left(\frac{1}{v_{\mathrm{g,e}}} - \frac{1}{v_{\mathrm{g,o}}}\right)^2 \tag{9}$$

Applicability to Various Wavelength Ranges

We will limit our experimental and theoretical study in this paper to second harmonic generation of Nd:YAG laser radiation with KDP and KD*P crystals. Both crystals have the property that, for type II second harmonic generation, the group velocity of the second harmonic is intermediate between the group velocities of the ordinary and extraordinary fundamentals. This property is unfortunately only found for the conversion of near-IR pulses. Fortunately, it has been shown that the combination of tilted energy fronts and angular walk-off between fundamental and second harmonic can be exploited to essentially tune the relative group velocities of the fundamental and second harmonic waves (17). Therefore, the results obtained for KDP in the near IR can be extended to a broad palette of wavelengths in the visible and IR.

The group velocities for the three waves (fundamental ordinary and extraordinary, second harmonic extraordinary) are given for KDP and KD*P in Table 1.

It is particularly intriguing that large pulse compression can be achieved, in spite of the following circumstances:

(1) The crystal length is close to the length corresponding to the phase-matching bandwidth required to support the femtosecond pulses that are generated.
(2) Group-velocity dispersion should affect also the shortest pulses that are generated.

The first point can be explained by the fast depletion of the fundamental. It is this fast amplitude modulation that provides the bandwidth required for the production of short pulses. The exact conditions for compression are not easily met—in fact, pulse broadening rather than compression has also been predicted and observed (18). The crystal length has to be accurately chosen. Ibragimov and Struthers (19) have shown

Table 1. Group velocities for the o, e, and second harmonic e waves. Values are calculated for type II second harmonic generation of 1.064 μm radiation.

Crystal	Fundamental (o) $v_{g,o}$ (cm/ps or 10^{10} m/s)	Second Harmonic (e) $v_{g,2}$ (cm/ps or 10^{10} m/s)	Fundamental (e) $v_{g,e}$ (cm/ps or 10^{10} m/s)
KDP	1.961×10^{-2}	1.984×10^{-2}	2.013×10^{-2}
KD*P	1.977×10^{-2}	1.984×10^{-2}	2.015×10^{-2}

that after complete crossing, the fundamental pulses can recover their energy, the second harmonic ultimately restituting its energy to the fundamentals. As pointed out by them, the equations in the time domain (neglecting group-velocity dispersion for each pulse) describe soliton crossing of the fundamental pulses.

The second point has never been addressed, because all models to date have been based on Maxwell's equation in the time domain, where group-velocity effects have to be treated by higher-order (than 1) differential operators. We present here an approach in the frequency domain, where the dispersion is taken exactly into account to any order. It will be seen that the influence of the higher-order terms is significant.

General Equations and Notation

Our model is based on equations presented in Ref. 20.

We derive the wave equation from Maxwell's equations in MKS units. For a total electric field vector $\boldsymbol{E}$, which will be the sum of the second-harmonic field polarized as an e wave and the fundamentals polarized as o and e waves, we get

$$\left(\frac{\partial^2}{\partial x^2}+\frac{\partial^2}{\partial y^2}+\frac{\partial^2}{\partial z^2}-\frac{1}{c^2}\frac{\partial^2}{\partial t^2}\right)\boldsymbol{E}(x,y,z,t)=\mu_0\frac{\partial^2}{\partial t^2}\boldsymbol{P}(x,y,z,t) \tag{10}$$

where μ_0 is the magnetic permeability of free space. The source term of Eq. (10) contains the polarization $\boldsymbol{P}$, which is decomposed into two parts:

$$\boldsymbol{P}=\boldsymbol{P}^{\mathrm{L}}+\boldsymbol{P}^{\mathrm{NL}} \tag{11}$$

For the linearly polarized plane wave propagating along z, the wave equation reduces to

$$\left(\frac{\partial^2}{\partial z^2}-\frac{1}{c^2}\frac{\partial^2}{\partial t^2}\right)\boldsymbol{E}(z,t)=\mu_0\frac{\partial^2}{\partial t^2}(\boldsymbol{P}^{\mathrm{L}}+\boldsymbol{P}^{\mathrm{NL}}) \tag{12}$$

Substituting for the Fourier-transformed linear polarization $\tilde{\boldsymbol{P}}^{\mathrm{L}}(\Omega, z) = \epsilon_0 \chi(\Omega)\tilde{\boldsymbol{E}}(\Omega, z)$ in the Fourier transform of the propagation Eq. (12), we have

$$\left(\frac{\partial}{\partial z} + i\frac{\Omega}{c}\epsilon(\Omega)\right)\left(\frac{\partial}{\partial z} - i\frac{\Omega}{c}\epsilon(\Omega)\right)\tilde{\boldsymbol{E}}(z, \Omega) = \mu_0 \Omega^2 \tilde{\boldsymbol{P}}^{\mathrm{NL}}(\Omega, z) \tag{13}$$

where we have introduced the dielectric constant

$$\epsilon(\Omega) = 1 + \chi(\Omega) \tag{14}$$

and the Fourier-transformed nonlinear polarization $\tilde{\boldsymbol{P}}^{\mathrm{NL}}(\Omega, z)$. Let us substitute for the total field $\boldsymbol{E}$ in the Fourier transform of Eq. (12):

$$\begin{aligned}\tilde{\boldsymbol{E}}(\Omega, z) &= \tilde{\boldsymbol{E}}_2(\Omega, z) + \tilde{\boldsymbol{E}}_{\mathrm{o}}(\Omega, z) + \tilde{\boldsymbol{E}}_{\mathrm{e}}(\Omega, z) \\ &= \tfrac{1}{2}\tilde{\mathscr{E}}_2(\Omega - \omega_2, z)e^{-ik_2(\Omega-\omega_2)z}\hat{\mathbf{1}}_{\mathrm{e}} \\ &\quad + \tfrac{1}{2}\tilde{\mathscr{E}}_{\mathrm{o}}(\Omega - \omega, z)e^{-ik_{\mathrm{o}}(\Omega-\omega)z}\hat{\mathbf{1}}_{\mathrm{o}} \\ &\quad + \tfrac{1}{2}\tilde{\mathscr{E}}_{\mathrm{e}}(\Omega - \omega, z)e^{-ik_{\mathrm{e}}(\Omega-\omega)z}\hat{\mathbf{1}}_{\mathrm{e}} + \mathrm{c.c.}\end{aligned} \tag{15}$$

where $\hat{1}_{\mathrm{o}}$ and $\hat{1}_{\mathrm{e}}$ represent unit vectors along the ordinary and extraordinary directions of polarization, and Ω is the frequency variable in the Fourier transform. In Eq. (15), the propagation constants $k_i(\Omega)$ are defined by

$$\begin{aligned}k_2(\Omega) &= \frac{\Omega}{c}\sqrt{\epsilon_2(\Omega)} = \frac{\Omega}{c}n_2(\Omega) \\ k_{\mathrm{o}}(\Omega) &= \frac{\Omega}{c}\sqrt{\epsilon_{\mathrm{o}}(\Omega)} = \frac{\Omega}{c}n_{\mathrm{o}}(\Omega) \\ k_{\mathrm{e}}(\Omega) &= \frac{\Omega}{c}\sqrt{\epsilon_{\mathrm{e}}(\Omega)} = \frac{\Omega}{c}n_{\mathrm{e}}(\Omega)\end{aligned} \tag{16}$$

The Fourier transforms of the fundamental fields $\tilde{\boldsymbol{E}}_{\mathrm{o}}$ and $\tilde{\boldsymbol{E}}_{\mathrm{e}}$ are centered at $\Omega = \omega$, and the Fourier transform of the second harmonic field $\tilde{\boldsymbol{E}}_2$ is centered at $\Omega = \omega_2 = 2\omega$. The total nonlinear polarization, in the time domain, has contributions at the second harmonic and fundamental wavelengths along the extraordinary direction, and one contribution at the fundamental wavelength along the ordinary wave:

$$\begin{aligned}\tilde{\boldsymbol{P}}^{\mathrm{NL}}(\Omega, z) = \epsilon_0 \chi^{(2)}[&E_{\mathrm{o}}(\Omega, z)E_{\mathrm{e}}(\Omega, z)\hat{\mathbf{1}}_{\mathrm{e}} \\ &+ E_2(\Omega, z)E_{\mathrm{o}}^*(\Omega, z)\hat{\mathbf{1}}_{\mathrm{e}} + E_2(\Omega, z)E_{\mathrm{e}}^*(\Omega, z)\hat{\mathbf{1}}_{\mathrm{o}}]\end{aligned} \tag{17}$$

It is straightforward to insert the total field (16) and the Fourier transform of the nonlinear polarization (18) into the propagation Eq. (13). One can decompose the resulting equation into a system of coupled equations, one corresponding to the spectral components around the second harmonic frequency, and the other two

corresponding to the ordinary and extraordinary components of the fundamental field:

$$\frac{\partial \tilde{\mathscr{E}}_2(\Delta\Omega,z)}{\partial z} = -i\frac{\omega_2\chi^{(2)}}{4n_2c}\int_{-\infty}^{\infty}\tilde{\mathscr{E}}_o(\Delta\Omega',z)\,\tilde{\mathscr{E}}_e(\Delta\Omega-\Delta\Omega',z) \times e^{-i[k_o(\Delta\Omega')+k_e(\Delta\Omega-\Delta\Omega')-k_2(\Delta\Omega)]z}\,d\Delta\Omega' \tag{18}$$

$$\frac{\partial \tilde{\mathscr{E}}_o(\Delta\Omega,z)}{\partial z} = -i\frac{\omega_2\chi^{(2)}}{4n_oc}\int_{-\infty}^{\infty}\tilde{\mathscr{E}}_2(\Delta\Omega',z)\,\tilde{\mathscr{E}}_e^{*}(\Delta\Omega'-\Delta\Omega,z) \times e^{-i[k_o(\Delta\Omega)+k_e(\Delta\Omega'-\Delta\Omega)-k_2(\Delta\Omega')]z}\,d\Delta\Omega' \tag{19}$$

$$\frac{\partial \tilde{\mathscr{E}}_e(\Delta\Omega,z)}{\partial z} = -i\frac{\omega_2\chi^{(2)}}{4n_ec}\int_{-\infty}^{\infty}\tilde{\mathscr{E}}_2(\Delta\Omega',z)\,\tilde{\mathscr{E}}_o^{*}(\Delta\Omega'-\Delta\Omega,z) \times e^{-i[k_e(\Delta\Omega)+k_o(\Delta\Omega'-\Delta\Omega)-k_2(\Delta\Omega')]z}\,d\Delta\Omega' \tag{20}$$

To simplify the notation, we have introduced $\Delta\Omega$ as argument of the Fourier transforms of the envelopes:

$$\begin{aligned}\tilde{\mathscr{E}}_2(\Delta\Omega,z) &= \tilde{\mathscr{E}}(\Omega-2\omega)\\ \tilde{\mathscr{E}}_o(\Delta\Omega,z) &= \tilde{\mathscr{E}}(\Omega-\omega)\\ \tilde{\mathscr{E}}_e(\Delta\Omega,z) &= \tilde{\mathscr{E}}(\Omega-\omega)\end{aligned} \tag{21}$$

Note that $\Delta\Omega$ in Eq. (18) covers a two times broader bandwidth than $\Delta\Omega'$. Similarly, $\Delta\Omega'$ in Eq. (19) and Eq. (20) cover two times the bandwidth of $\Delta\Omega$ in these equations.

The real group velocity is included in these expressions. It is convenient to present the solutions of the system of Eqs. (18), (19), (20) in the time domain, in a frame of reference propagating with a group velocity v_{g2}. The fields to be represented are given by

$$\tilde{\mathscr{E}}_2(t,z) = \int_{-\infty}^{\infty}\tilde{\mathscr{E}}_2(\Delta\Omega,z)e^{-i[k_2(\Delta\Omega)-k_2-\Delta\Omega/v_{g2}]z}e^{-i\,\Delta\Omega}\,d\Delta\Omega \tag{22}$$

$$\tilde{\mathscr{E}}_o(t,z) = \int_{-\infty}^{\infty}\tilde{\mathscr{E}}_o(\Delta\Omega,z)e^{-i[k_o(\Delta\Omega)-k_2-\Delta\Omega/v_{g2}]z}e^{-i\,\Delta\Omega}\,d\Delta\Omega \tag{23}$$

$$\tilde{\mathscr{E}}_e(t,z) = \int_{-\infty}^{\infty}\tilde{\mathscr{E}}_e(\Delta\Omega,z)e^{-i[k_e(\Delta\Omega)-k_2-\Delta\Omega/v_{g2}]z}e^{-i\,\Delta\Omega}\,d\Delta\Omega \tag{24}$$

The constant terms k_2, k_o, and k_e are the leading terms of the Taylor expansions for the wave vectors $k_2(\Delta\Omega)$, $k_o(\Delta\Omega)$, and $k_e(\Delta\Omega)$; v_g can be calculated from the Sellmeier equations. If we choose the frame of reference

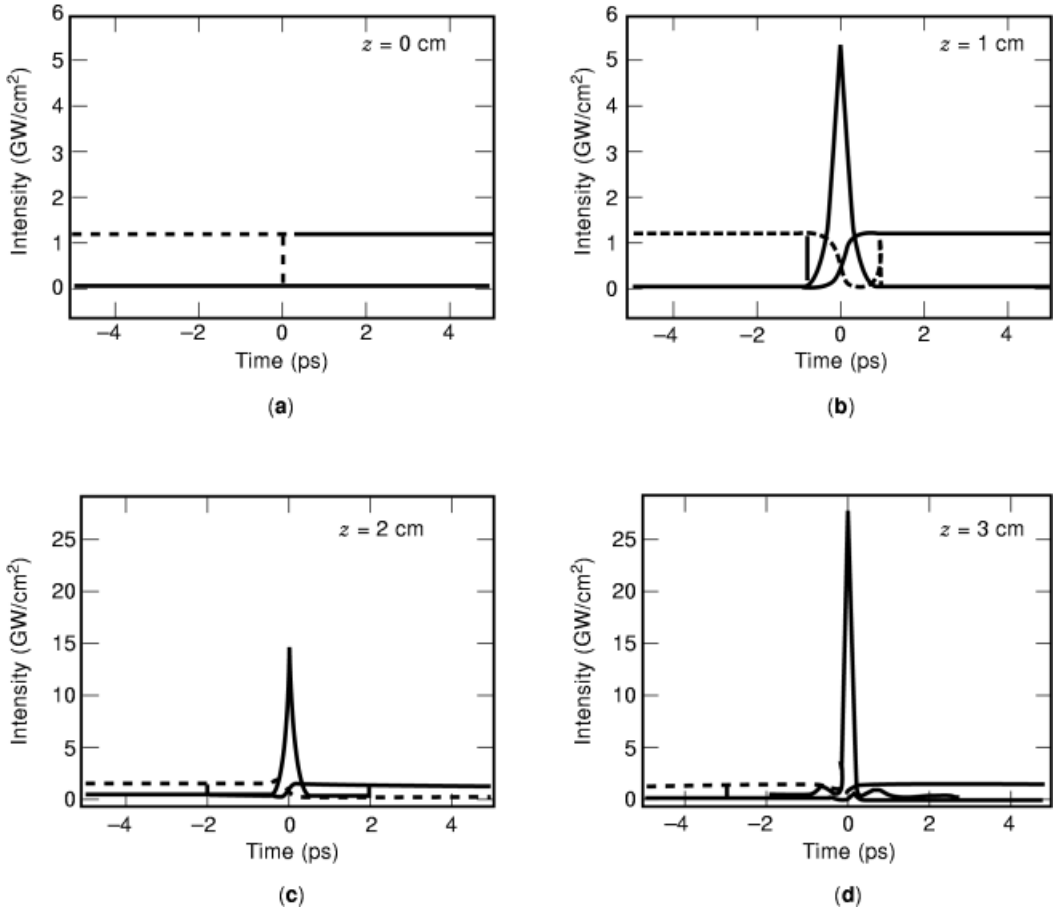

Fig. 3. Square-pulse second harmonic generation. The dotted and dashed lines are the ordinary and extraordinary fundamental intensities, respectively. The solid lines represent the extraordinary second harmonic intensity. The successive plots are for (a) $z = 0$ cm, (b) $z = 1$ cm, (c) $z = 2$ cm, (d) $z = 3$ cm. Note the different scales in intensity.

moving with the second harmonic pulse, then

$$\frac{1}{v_{g2}} := k_2'|_{2\omega} \tag{25}$$

Results of Numerical Simulations

The following simulations are based on second harmonic generation in KDP, where the full Sellmeier formulae have been used in the definition of the various k vectors that appear in the wave equations. As a result, our model takes into account *all* group-velocity dispersion effects as they affect the pulse propagation and the pulse conversion process. As an illustration of the simple analytical consideration of the section describing the

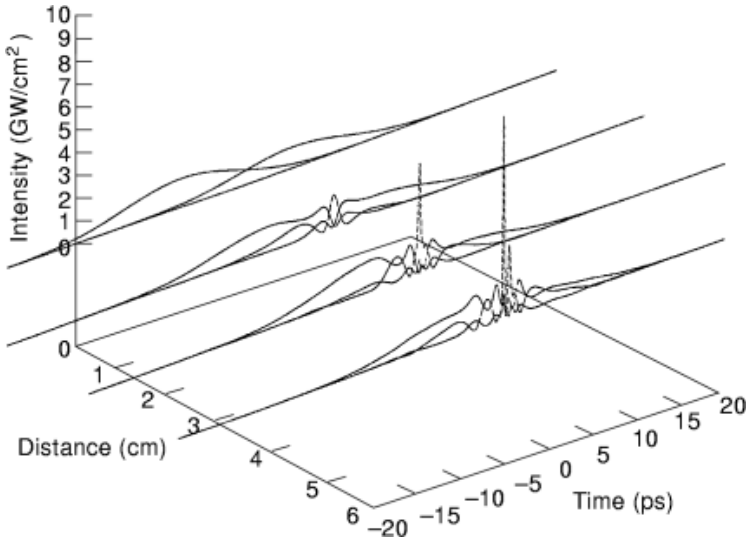

Fig. 4. Three-dimensional representation of the propagation of the fundamental and the second harmonic pulses.

model, we calculate the second harmonic generated by two step functions (temporal profile). Two step-function fundamental pulses enter the crystal with no initial overlap [Fig. 3(a)].

The ordinary and the extraordinary fundamental intensities are chosen to be equal, and the relative group velocities are also chosen to be equal but opposite in sign. A short pulse is generated after a distance of 1 cm, as shown in Fig. 3(b). In agreement with the simple considerations of the section describing the model, the width of the generated second harmonic is determined by the depletion of the two fundamentals moving into each other. The situation is much more complex when the full frequency dependence of the k vectors is taken into account. Perfect phase matching exists only for a single frequency component. Because of the frequency dependence of the wave vectors, there will be some transfer of energy back from the second harmonic to the fundamental.

Figures 4 and 5 illustrate the propagation and harmonic generation of two fundamental pulses with a gausian temporal profile. The fundamental ordinary and extraordinary waves have respectively intensities of 1.4 and 1 GW/cm^2, with the extraordinary wave being predelayed by 14 ps with respect to the ordinary wave. A three-dimensional representation of the propagation of the intensities of the three waves inside a 6 cm long KDP crystal is shown in Fig. 4. The depleted fundamental and second harmonic waves are shown after a propagation distance of 6 cm in Fig. 5(a) and 5(b). To assess the influence of group-velocity dispersion and higher-order terms in the expansion of the k vectors, the same calculation was performed in the approximation of constant group velocity at the various wavelengths. The results are shown in Fig. 5(c) and 5(d). The parameters of the calculation were chosen for optimum pulse compression in the complete model. The very large difference in conversion efficiency in the two cases clearly indicates that the higher-order terms in the expansion of the wave vector cannot be neglected.

Experimental Results

We have also carried out an experimental investigation of pulse compression. Our experimental arrangement, shown in Fig. 6, is similar to the arrangement described in Ref. 12.

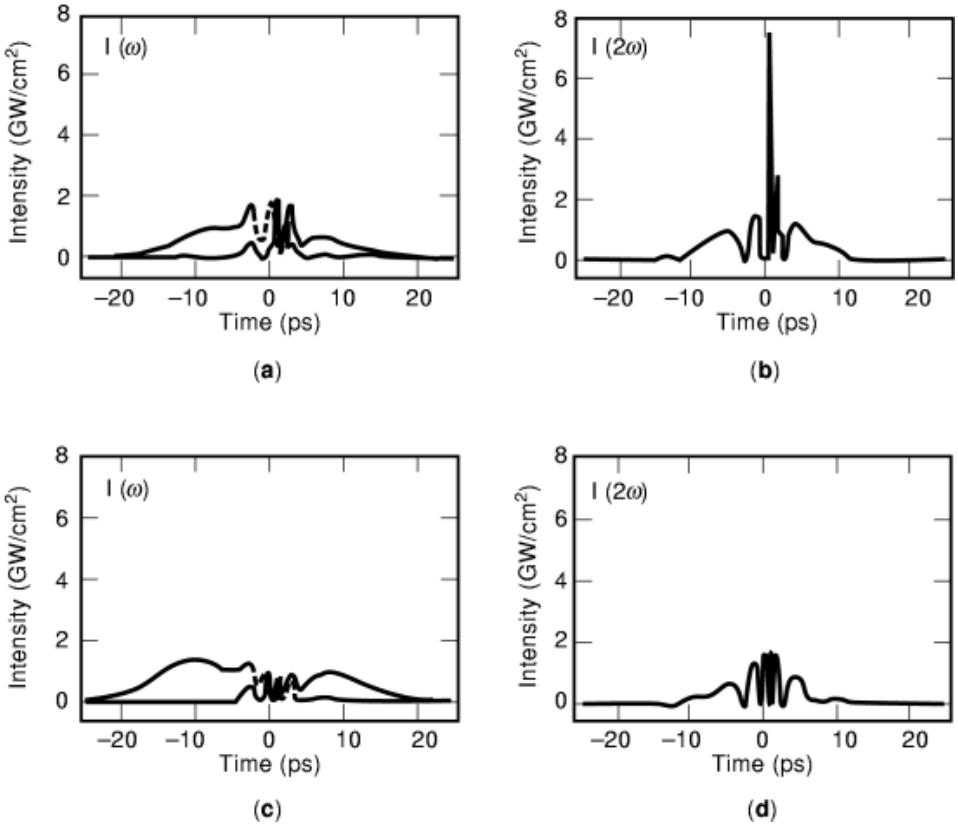

Fig. 5. Results of the numerical simulation for pulse shapes of fundamental and second harmonic pulses after propagation in 6 cm long KDP crystal. (a) and (b) correspond to the exact calculation, and (c) and (d) to the case of a linear approximation, neglecting group-velocity dispersion.

The pump source is an active-passive mode-locked Nd:YAG laser controlled by passive negative feedback (6). A single pulse of 0.2 mJ energy and 14 ps duration is extracted from the oscillator (a modified Continuum model PY61-10) and sent through two amplifiers. After the first (double-pass) amplifier with a 9 mm diameter Nd:YAG rod, the energy of the single pulse is 7 mJ, which is increased by the second amplifier (single pass) to the level of 50 mJ to 100 mJ. This second amplifier has a 12 mm diameter Nd:YAG rod, in order to minimize self-phase-modulation of the pulse spectrum. Spatial filtering and apodized apertures are used to ensure a uniform beam profile. The linearly polarized output beam passes through a half-wave plate, which rotates its plane of polarization by 45°. The beam is then separated into two components by a polarizing beamsplitter, and each component is given a relative delay before being recombined at a second polarizing beamsplitter. The rotation of the wave plate enables one to control the ratio between the energies of the two beams. The recombined pulses are sent as e and o waves into the second-harmonic-generating crystal (6 cm long KDP). A portion of uniform intensity at the beam center is selected by a 9 mm apodized aperture positioned just before the crystal.

The duration of the compressed pulses at the second harmonic frequency was measured with a single-shot autocorrelator based on noncollinear second harmonic generation in a 2 mm KDP type I crystal. An example of an autocorrelation trace of the second harmonic pulse, measured by a single-shot intensity autocorrelation, is shown in Fig. 7. The total power density of the 1.06 μm beam incident on the 6 cm long KDP crystal was 2.6

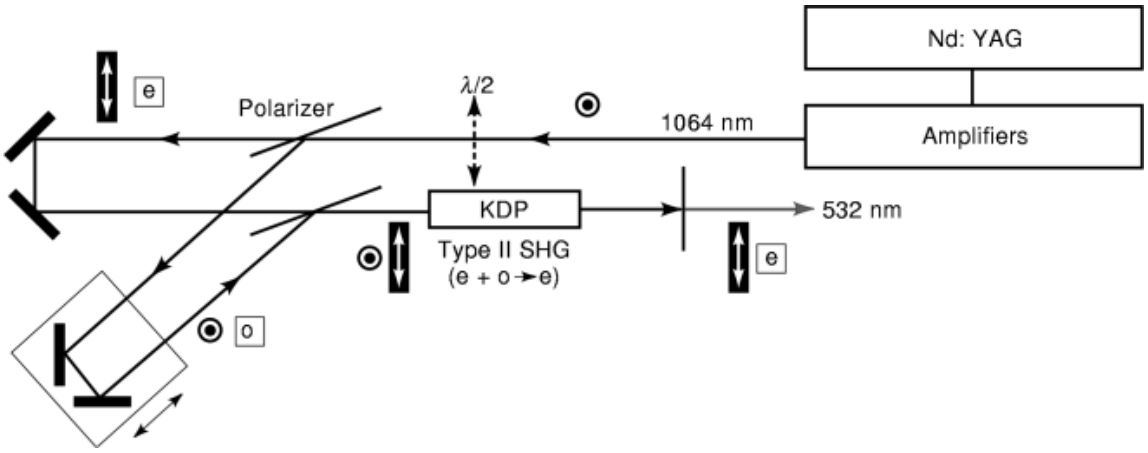

Fig. 6. Experimental setup.

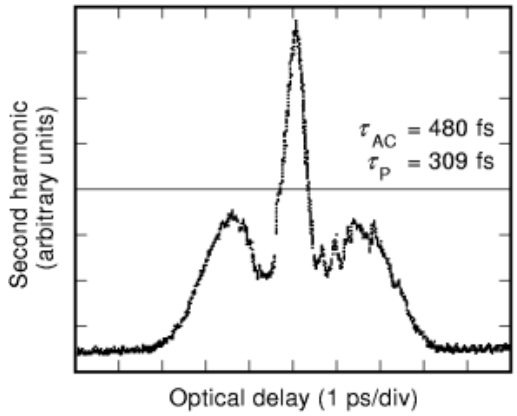

Fig. 7. Single-shot autocorrelation trace of a compressed 532 nm pulse. The time delay on the horizontal axis is 1 ps/div. The autocorrelation intensity is plotted in arbitrary units.

GW/cm^2. The fundamental e beam was given a predelay of 10.5 ps with respect to the o wave. The intensity of the o pulse was 1.3 times that of the e pulse. The conversion efficiency was 14%. The width of the autocorrelation curve of the (green) compressed pulse is 480 fs, which corresponds to a sech^2 pulse of 309 fs duration. The compression factor is thus 45.

The single-shot autocorrelator is a convenient diagnostic tool to optimize the laser. A trace such as in Fig. 7 is very sensitive to the quality of the optics used. For instance, the noise appearing on the right lobe of Fig. 7 is due to scratches on the filter (the autocorrelation should be exactly symmetric). In addition, the background is enhanced because of a contribution to the second harmonic from a nonuniform spatial beam structure. A better peak-to-satellite contrast is measured for a slightly longer pulse duration, using the autocorrelator in a scanning mode. Such a trace is plotted in Fig. 8. In the latter case, the intensity of the o pulse is 1.6 times that of the e pulse. All other parameters are the same as in the previous figure. In the case of Fig. 8, the conversion efficiency is 10%. The autocorrelation width corresponds to a sech^2 pulse of 660 fs duration.

The theoretical simulation led to a minimum compressed pulse duration of approximately 200 fs. The exact phase-matching condition for the central pulse wavelength was maintained for all numerical simulations. In

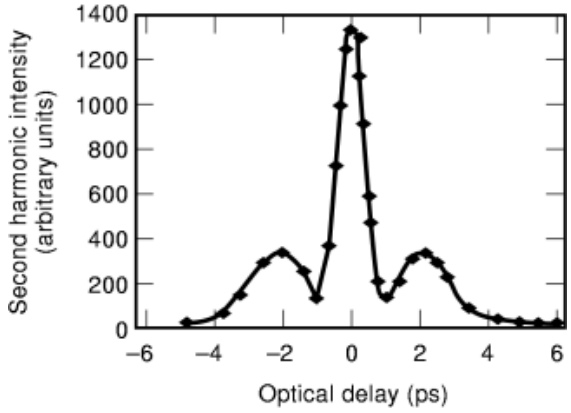

Fig. 8. Scanning autocorrelation trace of a compressed 532 nm pulse.

the actual experiment, the shortest pulses are obtained after a slight retuning of the long frequency doubling crystal. The two possible interpretations are that (1) the phase-matching condition is slightly different at high power than at low power, or (2) some dispersive effect of cascaded nonlinearities contributes to the pulse compression. Further simulations will be made in order to determine whether, within our theoretical model, optimum compression indeed occurs at some detuning from the low-power phase-matching condition.

Conclusion

In conclusion, we have shown that the pulse compression through type II second harmonic generation can lead to an intense femtosecond pulse source based on a flashlamp-pumped Nd:YAG laser. This frequency-doubled Nd:YAG laser is an ideal source for pumping amplifier stages of a synchronously pumped (femtosecond) parametric oscillator. Such a parametric oscillator can operate with a similar compression mechanism, and its output shows a structure similar to that of the compressed second harmonic: a main pulse with satellites. The presence of satellites will not be detrimental in that particular application, provided that the time delay between the main pulse and the satellites does not match for the 532 nm pump and the pulses to be amplified.

Acknowledgment

This work has been supported by the W. M. Keck Foundation, The National Science Foundation (ECS 9219450), and The Electrical Power Research Institute (RP 8610-01 and RP 5239-01).

BIBLIOGRAPHY

1. P. Maine *et al.*, Generation of ultrahigh peak power pulses by chirped pulse amplification, *IEEE J. Quantum Electron.*, **QE-24**: 398–403, 1988.
2. A. V. Babushkin *et al.*, Stable picosecond Nd:$YAlO_3$ crystal laser with hybrid mode-locking and passive intracavity feedback utilizing a GaAs crystal. *Sov. J. Quantum Electron.*, **19**: 1310–1311, 1989.
3. V. Kubecek *et al.*, Actively and passively mode-locked Nd:YAP($YAlO_3$) laser with negative feedback using CdSe and GaAs, *Jpn. J. Appl. Phys.*, **30**: L-1889–L1891, 1991.

4. V. Kubecek *et al.*, Self-defocusing of mode-locked Nd:YAG laser radiation in GaAs, CdSe and InP, *Jpn. J. Appl. Phys.*, **30**: L-1805–L1807, 1991.
5. T. F. Boggess Jr. *et al.*, Optical limiting in GaAs, *IEEE J. Quantum Electron.*, **QE-21**: 488–493, 1985.
6. A. Agnesi *et al.*, Generation of extended pulse trains of minimum duration by passive negative feedback applied to solid state q-switched lasers, *IEEE J. Quantum Electron.*, **28**: 710–719, 1992.
7. Y. Wang, R. Dragila, Efficient conversion of picosecond laser pulses into second-harmonic frequency using group-velocity-dispersion, *Phys. Rev. A*, **41**: 5645–5649, 1990.
8. A. Stabinis, G. Valiulis, E. A. Ibragimov, Effective sum frequency pulse compression in nonlinear crystals, *Opt. Commun.*, **86**: 301–306, 1991.
9. Y. Wang, B. L. Davies, Frequency-doubling pulse compressor for picosecond high power neodymium laser pulses, *Opt. Lett.*, **17**: 1459–1461, 1992.
10. P. Heinz *et al.*, Fiberless two-step parametric compression of sub-picosecond laser pulses, *Lithuanian Phys. Rev.*, **33**: 314–317, 1993.
11. A. Umbrasas *et al.*, Generation of femtosecond pulses through second harmonic compression of the output of a Nd:YAG laser, *Opt. Lett.*, **20**: 2228–2230, 1995.
12. A. Umbrasas *et al.*, Parametric oscillation and compression in KTP crystals, *Opt. Lett.*, **19**: 1753–1755, 1994.
13. J. D. V. Khaydarov, J. H. Andrews, K. D. Singer, Pulse compression in a synchronously pumped optical parametric oscillator from group-velocity mismatch, *Opt. Lett.*, **19**: 831–833, 1994.
14. J. D. V. Khaydarov, J. H. Andrews, K. D. Singer, 20-fold pulse compression in a synchronously pumped optical parametric oscillator, *Appl. Phys. Lett.*, **65**: 1614–1616, 1994.
15. L. Leford *et al.*, Generation of fs pulses from order of magnitude pulse compression in a cw synchronously pumped optical parametric oscillator, *CLEO '98*, San Francisco.
16. W. Koechner, *Solid-State Laser Engineering*, Berlin: Springer, 1996.
17. A. Dubietis *et al.*, Nonlinear second-harmonic pulse compression with tilted pulses, *Opt. Lett.*, **22**: 1071–1073, 1997.
18. D. A. Guk, V. G. Dmitirev, Some characteristics of second harmonic generation under conditions of strong energy exchange between interacting waves, *Kvantovaya Elektron.*, **18**: 106–110, 1990.
19. E. Ibragimov, A. Struthers, Second-harmonic pulse compression in the soliton regime, *Opt. Lett.*, **21**: 1582–1584, 1996.
20. J. C. Diels, W. Rudolph, *Ultrashort Laser Pulse Phenomena*, New York: Academic Press, 1995.

JENS BIEGERT
VACLAV KUBECEK
JEAN-CLAUDE DIELS
The University of New Mexico